Available online at www.sciencedirect.com
ScienceDirect
Journal of Magnetic Resonance 191 (2008) 231–238
JMR Journal of Magnetic Resonance
www.elsevier.com/locate/jmr

Design of a superconducting volume coil for magnetic resonance microscopy of the mouse brain ☆

John C. Nouls [a], Michael G. Izenson [b], Harold P. Greeley [b], G. Allan Johnson [a,*]

[a] *Center for In Vivo Microscopy, Duke University Medical Center, Box 3302, Durham, NC 27710, USA*
[b] *Creare Inc., Hanover, NH, USA*

Received 6 July 2007; revised 14 December 2007
Available online 5 January 2008

Abstract

We present the design process of a superconducting volume coil for magnetic resonance microscopy of the mouse brain at 9.4 T. The yttrium barium copper oxide coil has been designed through an iterative process of three-dimensional finite-element simulations and validation against room temperature copper coils. Compared to previous designs, the Helmholtz pair provides substantially higher B_1 homogeneity over an extended volume of interest sufficiently large to image biologically relevant specimens. A custom-built cryogenic cooling system maintains the superconducting probe at 60 ± 0.1 K. Specimen loading and probe retuning can be carried out interactively with the coil at operating temperature, enabling much higher through-put. The operation of the probe is a routine, consistent procedure. Signal-to-noise ratio in a mouse brain increased by a factor ranging from 1.1 to 2.9 as compared to a room-temperature solenoid coil optimized for mouse brain microscopy. We demonstrate images encoded at $10 \times 10 \times 20$ μm for an entire mouse brain specimen with signal-to-noise ratio of 18 and a total acquisition time of 16.5 h, revealing neuroanatomy unseen at lower resolution. Phantom measurements show an effective spatial resolution better than 20 μm.

Keywords: Superconducting coil; Microscopy; Mouse brain; Finite-element radiofrequency model; Helmholtz pair

1. Introduction

The fundamental resolution limits in biological magnetic resonance microscopy are defined by motion—macroscopic motion for live animal studies [1] and microscopic diffusion for tissue specimens [2–4]. A number of authors have acquired images at this diffusion-imposed limit, usually with specialized phantoms or over very limited fields of view where very small radiofrequency coils can be used to achieve the requisite sensitivity [3,5–7]. For larger specimens, the resolution limit is usually imposed by the limited signal from the smaller voxels. In 1984, Styles et al. [8] demonstrated that one can improve the signal-to-noise ratio of a spectroscopy experiment by cooling the coils, thus reducing the impact of thermal noise originating from the coil. Cryogenic copper probes have matured and are now commercially available for MRI [9,10]. Using a superconducting receiver, Hall et al. [11] imaged the back of a human head in 1991. Substantially higher SNR was demonstrated in microscopy by Black et al. in 1993 [12] using a yttrium barium copper oxide (YBCO)[1] coil. Since that time, a number of investigators have shown great progress towards a superconducting probe for routine MR microscopy [13–15], but the practical problems of radiofrequency inhomogeneity, tuning, matching, and cryogenic temperature

☆ Work supported in the United States in part by NIH/NIBIB (5 R44 EB000381), NIH/NIBIB (1 T32 EB001040), and performed at the Center for In Vivo Microscopy, an NCRR/NCI National Biomedical Technology Resource Center (P41 RR005959 and U24 CA092656). Additional support was provided by the Mouse Bioinformatics Research Network (U24 RR021760).
* Corresponding author. Fax: +1 919 684 7158.
E-mail address: gaj@orion.duhs.duke.edu (G.A. Johnson).

[1] *Abbreviations:* HTS, high-temperature superconducting; YBCO, yttrium barium copper oxide.

1090-7807/$ - see front matter © 2008 Elsevier Inc. All rights reserved.
doi:10.1016/j.jmr.2007.12.018

regulation have prevented the construction of reliable volume coils.

The design and construction of a superconducting probe are considerably more complex and expensive than traditional radiofrequency coils due to the special constraints imposed by the material and the need to maintain the coil at low temperature [16]. The superconducting film must be deposited on flat surfaces to achieve the crystalline structure required for superconductivity. The deposition of the film requires specialized expertise not available in most laboratories resulting in long turn-around time and high expense in the design cycle. A volume coil must be designed from an assembly of (at least two) coils and an associated coupling loop. Assembly of these very high Q resonators results in complex interactions that have profound impact on the homogeneity and final sensitivity. We describe here the design process that includes initial simulation using finite-element design tools, validation using more easily fabricated copper models, and final construction using high-temperature superconducting coils. We demonstrate the process and the validation of the models used to design our second generation of volume probe consisting of two spiral coils in Helmholtz pair configuration, inductively coupled to the radiofrequency chain. The $11 \times 11 \times 22$ mm volume coil is more homogeneous than previous probes. Agreement is very good in frequency and impedance between the finite-element model and both the superconducting and copper coils, providing a foundation for the design of future coils.

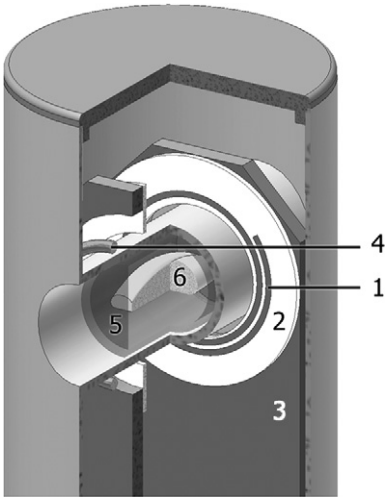

Fig. 1. The schematic shows the essential components of the HTS volume probe. A segment of the second HTS coil and heat exchanger is removed in this schematic to allow better appreciation of the geometry. The superconducting traces (1) are deposited on sapphire substrates (2) attached to beryllium oxide ceramic heat exchangers (3) in thermal contact with titanium chambers containing flowing helium vapor. The spacing between the heat exchangers can be adjusted to fine-tune the probe. The coils are inductively coupled to the radiofrequency chain by an untuned room-temperature circular copper coupling loop (4) which can slide along the axis of the pair to adjust the power match. The cartridge (5) containing the mouse brain (6) is placed at the center of the Helmholtz pair. Vacuum is actively maintained inside the probe housing to limit heat convection towards the cold coils. A flow of room-temperature nitrogen prevents the sample from freezing during operation. A copper foil is wrapped around the probe housing and acts as a radiofrequency shield.

2. Simulations

We have used finite-element methods to describe the coil, starting with individual elements, moving to more complex assemblies of these elements, and finally expanding to consider more subtle effects of dielectric losses and coupling to the radiofrequency shield. To maximize the region of high B_1 field homogeneity, given the requirement that the HTS material has to be deposited on a flat substrate, we choose a pseudo-solenoid construction consisting of two spiral coils and one coupling loop. The two spiral coils are parallel with each other and the coupling loop, with the spiral centers aligned on the same axis (Fig. 1).

One of the initial challenges is tuning the HTS coils to the desired Larmor frequency. Our previous work [13] employed a complex thin film pattern with distributed capacitance and inductance between the elements of the thin film, which was difficult to tune. Withers et al. [17] and Serfaty et al. [18] presented double-sided spiral coils. For this work, we selected a single-sided spiral coil (Fig. 2). Tuning the individual coils is easily achieved by scribing a line through the YBCO material to reduce the total length of the spiral. Several methods have been presented to calculate the resonant frequency of spiral coils and the frequency shift within a Helmholtz pair [19–21]. Finite-element methods can achieve the same purpose when the wavelength of interest is within a few orders of magnitude of the physical dimension of the coil. They offer the supplementary ability to model complex components, including the radiofrequency shield or elaborate dielectric material geometries. The resonant frequency of the individual, stand-alone spiral was determined by finite-element simulation as a function of average diameter and pitch of the spiral, as well as width of the conductor and number of turns. Our target was approximately 400 MHz for coil dimensions appropriate to image a mouse brain. The full-wave three-dimensional electromagnetic simulations of the single spiral coil, as well as the empty and specimen-loaded probe, including the radiofrequency shield and the dielectric ceramic heat exchangers, were performed using a commercially available finite-element software (HFSS version 9.1, Ansoft Corporation, Pittsburgh, PA). Electromagnetic properties of materials were obtained from literature. No model of superconductivity was implemented; a conductivity of 10^{12} (S/m) was used for the superconducting material. A conductivity of 1 (S/m) and a permittivity of 50 were used for the specimen. The convergence criteria were chosen to guarantee a precision better than 2%. A typical simulation was complete within a few hours using a standard personal computer (3 GHz single processor, Dell Inc., Round Rock, TX).

Loading a specimen into the probe causes a frequency shift that requires fine tuning. A ceramic wedge inserted

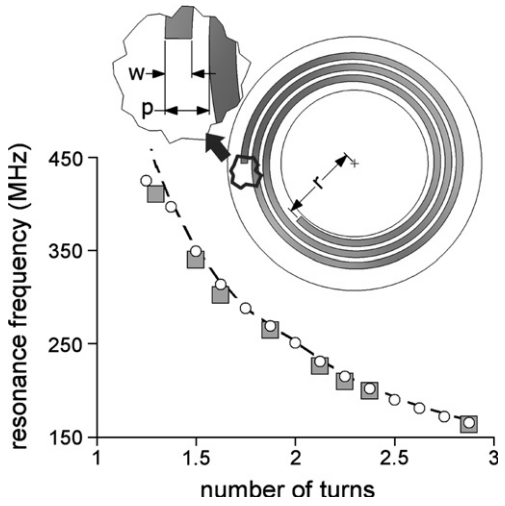

Fig. 2. A detailed view of one coil of the Helmholtz pair shows the pitch p of a spiral, and the trace width w. The inner radius r of the coil is measured to the midline of the inner trace. The spiral coil parameters are: $r = 11.75$ mm, $w = 1$ mm and $p = 1.65$ mm. The substrate is a 38 mm outer diameter, 22 mm inner diameter, one-millimeter thick sapphire ring. Each coil resonates at 180 MHz as manufactured with an original number of turns of $N = 2.875$. It can be brought to 410 MHz by reducing the number of turns to approximately 1.3, in which case the coil average radius is $a = 12.9$ mm. During manual tuning, a segment at the outer end of the coil trace can be isolated from the part supporting the resonant mode by making a score with a razor blade. The number of turns carrying the resonant mode, the inductance and the capacitance are decreased and the resonant frequency increases. The isolated, unused segment of trace is left on the substrate. Data from a copper replica (○) is compared to tuning data from a superconducting coil after its manufacturing (□), as well as simulations (dashed line).

Fig. 3. A photograph of the copper replica of the superconducting probe shows that the geometry of the copper coils is identical to that of the superconducting coils. The relative dielectric constant (10) of the organic ceramic substrate of the copper laminate is very close to that of the sapphire substrate (11) of the superconducting coils. The acrylic support allows one to adjust the relative position of the coils in the same fashion as the HTS probe and experimentally validate the radiofrequency simulations of the superconducting probe.

between the coils allows one to adjust the separation between the coils while they are cold. As one might expect, this affects the B_1 homogeneity [21] and the power match. Simulations were conducted to determine the resonant frequency, the apparent impedance, and the field homogeneity of the loaded, shielded probe for a displacement between the two main coils ranging from 12.5 to 15 mm. A separation distance between the coils of 12.9 mm corresponds to a Helmholtz pair.

The simulations were validated using a room temperature replica with individual copper coils (Fig. 3). Spiral coils with trace width, spacing, and pitch identical to the HTS coils were machined from a copper laminate (CER-10 laminate, Taconic ADD, Petersburgh, NY), which has a relative dielectric constant of 10, very close to that of the sapphire substrate, equal to 11, used with the HTS coils.

3. Experiments

After the completion and validation of the simulations, HTS coils were fabricated by deposition of a 300 nm-thick, epitaxially grown yttrium barium copper oxide film (Theva GmbH, Ismaning, Germany) on a low dielectric loss sapphire substrate, passivated with a 100 nm-thick gold layer. These coils form the basic elements of our second generation of volume probe shown schematically in Fig. 1. The two superconducting coils were bonded to one end of heat exchangers made out of beryllium oxide, a ceramic chosen for its high thermal conductivity and low loss tangent. The other end of the heat exchangers was bonded to titanium chambers containing the flow of cryogenic vapor. The cylindrical body of the probe was machined from a garolite hollow tube, around which a room-temperature, one thousandth of an inch thick, copper shield was wrapped. Vacuum is actively maintained by a turbomolecular pump (Turbovac 361, Oerlikon Leybold Vacuum, Cologne, Germany) in a custom-built Gifford-McMahon cycle cryocooler (Creare Inc., Hanover, NH). Cooling the probe is a routine procedure that requires 4 h. The cryocooler is linked to the superconducting probe by a flexible, superinsulated vacuum line carrying a stream of cryogenic helium vapor circulating to and returning from the probe. The flexible coupling allows the probe to be removed from the magnet and the specimen to be changed without warming the probe. Temperature feedback controls the power input to a small heater just upstream from the titanium chambers at the base of the probe. The arrangement maintains the probe at 60 ± 0.1 K over cold runs lasting 96 h or more, limiting changes in coil quality factor and resonant frequency caused by temperature fluctuations [22].

Using the superconducting probe, field homogeneity profiles were recorded from an 11 mm diameter, 23 mm

long cylindrical phantom filled with silicone oil for comparison to predictions made by the radiofrequency model. A 3D gradient recalled sequence was used to eliminate the impact of nonlinearity [26] in the refocusing pulse of the more traditional rf refocused sequence. The same image acquisition was repeated using the room-temperature replica. In both cases, the power level of a hard pulse exciting the entire phantom was chosen such as to maximize the signal intensity at the center of the pair. Signal-to-noise measurements were made at multiple points in the imaging volume.

Three-dimensional imaging at very high spatial encoding resolution requires a dynamic range beyond that of our 16-bit analog-to-digital converter [28] . A three-dimensional Cartesian spin warp encoding scheme was implemented with accompanying reconstruction software to accommodate image arrays up to 4096^3. The scheme extends the dynamic range of the spectrometer by breaking Fourier space into smaller volumes. The gain of the amplifier immediately in front of the 16-bit analog-to-digital converter is set separately for each of the subvolumes of Fourier space. In the peripheral regions of Fourier space where the signal is low, the gain is increased to limit quantization errors. As the acquisition progresses toward the central volumes of Fourier space, the gain of the amplifier is reduced in 6 dB increments. At each increment, the number of excitations is doubled. Data is accumulated into 32-bit words, both for the real and imaginary channels.

Using the superconducting probe, gradient-recalled images were acquired of a perfusion-fixed C57BL/6 mouse brain, actively stained by transcardial perfusion with a mixture of 10% buffered formalin and ProHance (Bracco S.p.A., Milano, Italy) [23,24] allowing the use of short repetition time (TR $\leqslant$ 100 ms). Acquisition parameters were: GRE, Flip angle = 90°, TR = 100 ms, TE = 5.5 ms, FOV = 21.3 × 10.6 × 10.6 mm, Bandwidth = 62.5 kHz, NEX = 1, Voxel Size 10 × 10 × 20 μm, array size = 1024^3, 75% *k*-space asymmetric sampling. The total imaging time was 16.5 h. The same parameters were used to acquire data from another brain with a conventional room-temperature solenoid coil (14 mm diameter and 28 mm length), in which the filling factor was maximized for mouse brain microscopy. For each probe, signal-to-noise measurements were made from 3D gradient recalled images at multiple points in the imaging volume.

For the superconducting probe, the experimental quality factors Q_u of the empty probe, as well as the quality factor Q_L of the probe loaded with a mouse brain specimen, were recorded at operating field using two small (<1 cm), decoupled loops and a transmitted power S_{12} measurement [25] on a network analyzer (model 4195A, HP, Palo Alto, CA). Care was taken to limit the output power of the network analyzer so that the superconducting coil did not approach saturation [26]. For the room-temperature copper replica, the unloaded and loaded quality factors were recorded through the matched, untuned coupling loop circuit from the reflected power S_{11} on the network analyzer. Finally, using the same S_{11} method, the quality factor of the empty room-temperature solenoid probe, as well as the quality factor of the same probe loaded with a mouse brain, were recorded.

To test the in-plane resolution, a 50-μm-thick polyester mesh (Small Parts, Miami Lakes, FL) with an opening size of 20 μm immersed in a 0.05 M copper sulfate solution was imaged using the same sequence as was employed with the actively stained brain.

All images were acquired on a 9.4 T 89 mm vertical bore magnet (Oxford Instruments, Oxon, United Kingdom) interfaced to an imaging console (EPIC 12.0, General Electric Medical Systems, Milwaukee, WI) that has been modified for MR microscopy. Shielded coils provide gradients of 850 mT/m. The superconducting probe is connected to the spectrometer by a custom-designed T/R switch and preamplifier hybrid (Nova Medical, Wilmington, MA). The noise figure of the preamplifier, including all the connectors to the probe, was 0.6 dB. An intermediate stage in the radiofrequency transmit/receive chain mixes the 64 MHz operation frequency of the system designed originally for operation at 1.5 T with the signal from an independent oscillator to produce a sum signal at 400 MHz. Special care has been taken to ensure that this up/down converter, the preamplifier, and the first stage of the spectrometer can all accommodate the maximum amplitude of the signal from the superconducting probe without saturation effects.

4. Results

Fig. 2 shows the resonant frequency of the individual HTS coils as a function of the number of turns of the spiral. The final spiral structure with width (w) of 1 mm and pitch (p) of 1.65 mm provides an operating range of nearly 300 MHz as the number of turns is decreased from 3 to 1.2. In addition, precise adjustment of the final frequency does not require inordinate precision in the placement of the last score. The frequency is not linearly dependent on the length of the spiral; at 400 MHz, one can shift the center frequency by 5.3 MHz by removing ~1 mm of the trace so the final tuning is readily accomplished manually under a simple dissecting microscope.

The separation of the two HTS coils can be adjusted from 12.5 to 15 mm to provide fine tuning, while the coils are at operating temperature. Fig. 4 shows theoretical and experimental data for both the resonant frequency and impedance as a function of coil separation. The individual coils were tuned to 410 MHz. In the Helmholtz configuration, changing the separation from 12.5 to 15 mm resulted in a frequency shift from 400.1 to 403.3 MHz when loaded with a mouse brain inside our 9.4 T magnet (the Larmor frequency of hydrogen within our magnet is 400.2 MHz). The 50-Ω match was realized with the 22-mm diameter untuned coupling loop placed 20 mm away from the pair center. Fine tuning by adjusting the separation distance between the coils minimally alters the 50-Ω match: the

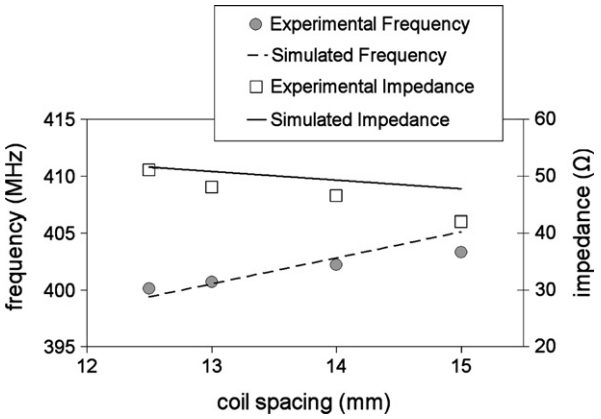

Fig. 4. A plot of resonant frequency and impedance for the coil pair vs separation shows the experimentally measured resonant frequency of the probe (●) varies from 400.1 to 403.3 MHz when loaded with a mouse brain. The total tuning range is 3 MHz. The dashed line shows the results of simulations of the probe resonant frequency. The experimental impedance of the probe (□) varies from 51 to 42 Ω and is compared to simulated data (solid line).

apparent impedance of the probe is 42 Ω at a 15 mm coil spacing.

In Fig. 5b, field homogeneity profiles acquired from the superconducting probe indicate that the signal intensity decreases by less than 14% over an 11 mm wide region on the center-plane perpendicular to the pair axis. Data acquired along the A/P axis is similar to the S/I axis (not shown). Along the pair axis in the R/L direction (Fig. 5a), signal intensity increases from a minimum at the pair center to +25% near the center of the left coil, and reaches a peak at +80% close to the center of the right coil. The signal does not decrease to a value lower than the minimum at the pair center over a 23 mm span. The holding field is parallel to the A/P axis.

Two different signal-to-noise ratio comparisons were made. The first comparison was made between the HTS and copper Helmholtz using the non-conductive silicon phantom. The unloaded quality factor of the probe at 9.4 T is 4800. A similar measurement for the copper replica yielded $Q_u = 320$. Signal-to-noise ratio, averaged over the entire longitudinal slice of the non-conducting sample (Fig. 5b) increased from 220 in the copper Helmholtz to 712 in the superconducting probe, an improvement of 3.2. The SNR in the brightest region of Fig. 5b (at R/L position of ~+10 mm) was 965 relative to 224 at the same point in the copper Helmholtz, a net increase of a factor of 4.2. The minimum SNR at R/L = 0 was 546 relative to 224 in the copper Helmholtz, a net increase of 2.4 for the HTS coil.

A second comparison of SNR was made between the HTS Helmholtz and the copper solenoid using a conducting sample, i.e. the perfused mouse brain. For the superconducting probe, the loaded quality factor (with the perfused brain) is 1800. Similar measurements for the copper solenoid yielded $Q_u = 420$ and $Q_L = 260$. In the images of the mouse brain, the signal-to-noise ratio increased in the HTS coil by a factor 1.9 in the hippocampus, 1.3 in the central lobe of the cerebellum, 1.1 in the uvula, and 2.9 in the frontal lobe using the superconducting probe relative to the same points in the brain images acquired with the copper solenoid.

Fig. 6 shows a single transverse slice of a polyester mesh immersed in copper sulfate imaged with a 1024^3 array. The effective slice is 20 μm. The in-plane resolution is 10 × 10 μm. The intersection of the imaging plane with the plane of the mesh is not perfect so volume averaging reduces the contrast in some parts of the image. The magnified inset shows areas in which the mesh is clearly resolved, as well as an intensity profile perpendicular to some mesh fibers.

Three-dimensional images of the entire mouse brain immersed in a hydrogen-free perfluoropolyether (Fomblin, Solvay Solexis S.p.A., Bollate, Italy) were acquired at 10 × 10 × 20 μm in 16.5 h. We believe these to be the highest resolution MR images of the mouse brain yet published,

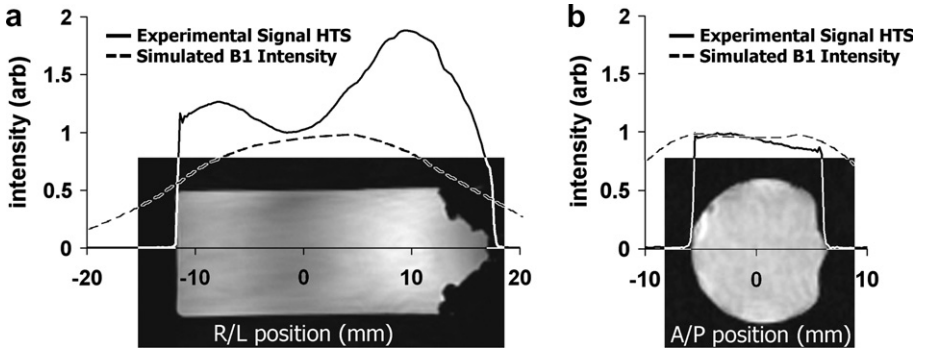

Fig. 5. Data from 3D isotropic images shows the signal intensity from a homogeneous cylindrical phantom, 11 mm in diameter an d 23 mm in length (excluding the lateral lid protrusion) filled with silicone oil. (a) Central longitudinal slice from the 3D array acquired with the HTS coil and signal intensity across the R/L direction for the HTS coil (solid line), through the center of the Helmholtz pair. The simulated B_1 field intensity is given by the dashed line. The coupling loop of the superconducting probe is located at position +20 mm along the R/L axis. The element closer to the coupling loop, located at +6.5 mm, carries more current and generates a higher B_1 field than the coil further away, placed at −6.5 mm. (b) signal intensity across the A/P direction for the HTS coil (solid line) through the center of the Helmholtz pair, and simulated B_1 field intensity (dashed line). The imaging parameters are: GRE 90°, TR 500 ms, TE 5.5 ms, FOV 51.2 × 25.6 × 25.6 mm, Bandwidth 62.5 kHz, NEX 1, Voxel Size 200 × 200 × 200 μm.

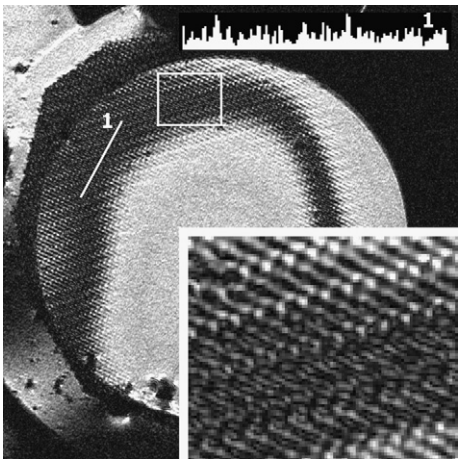

Fig. 6. Image of an octagonal piece of mesh fabric, clamped in a polymeric round clip, and immersed in copper sulfate (0.05 M) acquired with the superconducting probe. From a 1024^3 array, the selected imaging plane intersects the mesh with 20-μm openings along an arc on the left side of the image. The magnified section emphasizes dark regions of signal void delineating the mesh fibers. Bright dots mark the location of the mesh openings. The insert in the top-right corner shown the intensity profile acquired along line 1 placed perpendicular to the fibers. Two-pixel-wide peaks correspond to the position of the mesh openings falling within the imaging plane.

revealing anatomical features not seen in previous MR images. A representative coronal section through the hippocampus is compared to a histological section at the same level in Fig. 7. Note in Fig. 7a that fiber tracts are readily resolved in the caudate putamen. In the magnified area (Fig. 7b) one can resolve layers in the corpus collosum that are the thickness of only 3–4 cells in the accompanying optical section.

5. Discussion

We have developed a finite-element model to understand the critical design elements of an HTS coil. The radiofrequency model has allowed us to study the individual elements of our coil, e.g accurately predicting the resonant frequency of an individual spiral as a function of trace width, spacing, and total length. Agreement between the radiofrequency simulations and experiment is within 10% for the frequency of a single spiral over its entire tuning range spanning 300 MHz (Fig. 2). The model includes interactions between the individual coils and the coupling loop and allows us to determine frequency shifts and rf homogeneity as a function of coil separation- critical for the final stages of tuning and matching. The model agreed within 1% for the frequency over the 12–15 mm spacing of the coils. During imaging in practice, the probe resonant frequency at operating field typically decreases by less than 0.25 MHz when a mouse brain specimen is inserted into the probe and can be easily compensated with the 3 MHz fine-tuning range provided by the mechanical displacement of the two coils (Fig. 4).

The B_1 field homogeneity for the Helmholtz pair is superior to previous HTS coils. The inhomogeneity in the plane

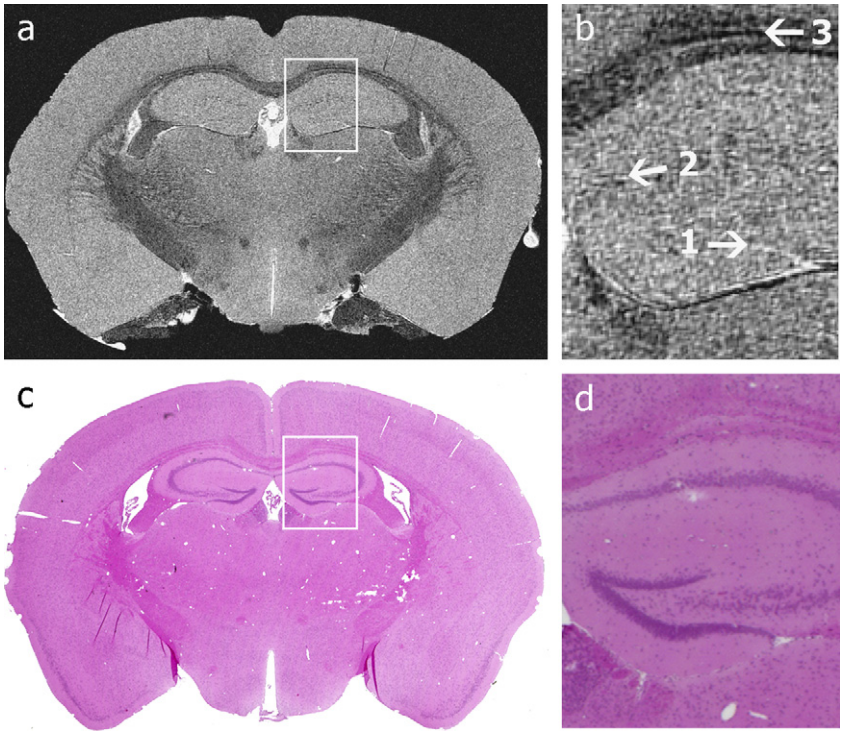

Fig. 7. (a) 20-μm thick transverse slice through the mouse hippocampus, at a 10-μm in-plane resolution. Both axes are phase-encoded. (b) In the hippocampus, transitions between layers (1 and 2) are visible. The layering of the corpus callosum (3) is apparent. Signal-to-noise ratio is 18. (c and d) Hematoxylin and eosin histological section of a different brain at approximately the same location, for comparison.

transverse to the axis of the coils is less than 14%. Along the axis of the coils, more pronounced B_1 inhomogeneity (Fig. 5) has been recorded, which was underestimated by our model. The replication of the analysis presented by Serfaty et al. [21] without shield or loading indicates that a negligible current imbalance between coils is due to the lateral position of the coupling loop. However, the shield decreases the coupling factor between coils in practice, and the current imbalance can be underestimated. Our finite-element model includes the shield; the B_1 inhomogeneity was nonetheless underestimated. The conductivity of each of the superconducting films may be different in practice whereas our radiofrequency model assumes equality. In addition, the relation between simulated B_1 intensity and measured MR signal may not be straightforward. A practical remedy consists of placing the loop on the mid-plane between the coils in order to equilibrate mutual inductance. Power transfer could be adjusted by sliding the loop slightly away from the mid-plane. The radiofrequency simulations allows us to easily explore alternative solutions.

For a non-conductive specimen, SNR is proportional to $\sqrt{\eta Q/T}$, where η is the filling factor and T is the noise temperature of the probe. We assume that the superconducting probe and the copper replica exhibit the same filling factor, and that the noise temperature of the copper Helmholtz is known to be room-temperature. A simple analysis of the maximum SNR increase of 4.2 between the two probes indicates that the noise temperature of the superconducting probe is 250 K.

For a conducting specimen, SNR increased by a factor ranging from 1.1 to 2.9 using the superconducting probe as compared to a copper solenoid. The filling factor of the superconducting probe is approximately 40% of that of the copper solenoid. Despite this difference, the HTS coil provides a significant gain in SNR.

The increase in sensitivity provided by the HTS coil allows us to encode at what we believe to be the highest resolution yet achieved for large-size biological specimens [27]. Spatial resolution of better than 20 μm was verified via the Raleigh criterion using a nylon mesh and in-plane encoding of 10×10 μm. Images of a perfusion fixed mouse brain at $10 \times 10 \times 20$ μm revealed clear distinction of layers approximately four cells thick.

6. Conclusion

To date, the use of HTS coils has been of limited value for MR microscopy. Challenges in designing a superconducting probe have restricted the extent of the field-of-view and the rf homogeneity has been poor, limiting the type of biological specimens that might be studied. The use of finite-element radiofrequency simulations enabled an easier and more cost-effective design process resulting in vastly improved radiofrequency homogeneity over larger field-of-views. The tuning and matching requirement were correctly predicted. Homogeneity was well modeled in the transverse plane. Our model underestimated the amplitude of the inhomogeneity along the axis of the pair, which can be alleviated in practice.

The probe filling factor can be improved. The finite-element simulations should be extended to include an energy-based estimation of the probe filling factor, and an estimation of power loss in the shield. A suitable shield configuration and the optimal trade-off between homogeneity and sensitivity can be determined by the model before implementing changes.

Extensive work is in progress to define the magnetic resonance and histological correlates of the mouse brain cytoarchitecture.

With useful guidance early in the probe design phase, we believe that routine MR microscopy of larger, biologically relevant specimens at a resolution approaching the limit imposed by water diffusion can be successfully implemented in the next 1–2 years.

Acknowledgments

The authors wish to thank the anonymous reviewers for their constructive suggestions, Wil Fisher and Andy Hopkins for installing the cryocooler, Boma Fubara for specimen preparation, Alexandra Badea for interpreting neuroanatomy, Gary Cofer and Brett Guenther for advice and useful conversations.

References

[1] W. Mai, C.T. Badea, C.T. Wheeler, L.W. Hedlund, G.A. Johnson, Effects of breathing and cardiac motion on spatial resolution in the microscopic imaging of rodents, Magnetic Resonance in Medicine 53 (2005) 858–865.

[2] P.T. Callaghan, C.D. Eccles, Diffusion-limited resolution in nuclear magnetic-resonance microscopy, Journal of Magnetic Resonance 78 (1988) 1–8.

[3] Z.H. Cho, C.B. Ahn, S.C. Juh, H.K. Lee, R.E. Jacobs, S. Lee, J.H. Yi, J.M. Jo, Nuclear magnetic-resonance microscopy with 4-Mu-M resolution—theoretical-study and experimental results, Medical Physics 15 (1988) 815–824.

[4] Z.H. Cho, C.B. Ahn, S.C. Juh, J.M. Jo, R.M. Friedenberg, S.E. Fraser, R.E. Jacobs, Recent progress in NMR microscopy towards cellular imaging, Philosophical Transactions of the Royal Society of London Series A-Mathematical Physical and Engineering Sciences 333 (1990) 469–475.

[5] L. Ciobanu, D.A. Seeber, C.H. Pennington, 3D MR microscopy with resolution 3.7 μm by 3.3 μm by 3.3 μm, Journal of Magnetic Resonance 158 (2002) 178–182.

[6] R.E. Jacobs, S.E. Fraser, Magnetic-resonance microscopy of embryonic-cell lineages and movements, Science 263 (1994) 681–684.

[7] S.C. Lee, K. Kim, J. Kim, S. Lee, J.H. Yi, S.W. Kim, K.S. Ha, C. Cheong, One micrometer resolution NMR microscopy, Journal of Magnetic Resonance 150 (2001) 207–213.

[8] P. Styles, N.F. Soffe, C.A. Scott, D.A. Cragg, F. Row, D.J. White, P.C.J. White, A high-resolution NMR probe in which the coil and preamplifier are cooled with liquid-helium, Journal of Magnetic Resonance 60 (1984) 397–404.

[9] R. Haueisen, D. Marek, M. Sacher, K. Ugurbil, S. Junge, Flexible cryoprobe-setup for mice brain imaging and spectroscopy at 9.4 T, in:

23rd Annual Scientific Meeting of the European Society for Magnetic Resonance in Medicine and Biology, Warsaw, Poland, 2006, pp. 78.
[10] N. Radzwill, R. Haueisen, D. Marech, M. Sacher, S. Junge, Benefits og cryogenic coils for routine in vivo mouse brain imaging and spectroscopy at 9.4 T, in: I.S.f.M.R.i. Medicine, (Ed.), ISMRM 15th Scientific Meeting and Exhibition, Berlin, Germany, 2007, pp. 627.
[11] A.S. Hall, N.M. Alford, T.W. Button, D.J. Gilderdale, K.A. Gehring, I.R. Young, Use of high-temperature superconductor in a receiver coil for magnetic-resonance-imaging, Magnetic Resonance in Medicine 20 (1991) 340–343.
[12] R.D. Black, T.A. Early, P.B. Roemer, O.M. Mueller, A. Mogrocampero, L.G. Turner, G.A. Johnson, A high-temperature superconducting receiver for nuclear-magnetic-resonance microscopy, Science 259 (1993) 793–795.
[13] S.E. Hurlston, W.W. Brey, S.A. Suddarth, G.A. Johnson, A high-temperature superconducting Helmholtz probe for microscopy at 9.4 T, Magnetic Resonance in Medicine 41 (1999) 1032–1038.
[14] H.L. Lee, I.T. Lin, J.H. Chen, H.E. Horng, H.C. Yang, High-T-c superconducting receiving coils for nuclear magnetic resonance imaging, IEEE Transactions on Applied Superconductivity 15 (2005) 1326–1329.
[15] F. Odoj, E. Rommel, M. von Kienlin, A. Haase, A superconducting probehead applicable for nuclear magnetic resonance microscopy at 7 T, Review of Scientific Instruments 69 (1998) 2708–2712.
[16] L. Darrasse, J.C. Ginefri, Perspectives with cryogenic RF probes in biomedical MRI, Biochimie 85 (2003) 915–937.
[17] R.S. Withers, G.C. Liang, B.F. Cole, M. Johansson, Thin-film HTS probe coils for magnetic-resonance imaging, Chicago, IL, USA, 1993, pp. 2450–2453.
[18] S. Serfaty, N. Haziza, L. Darrasse, S. Kan, Multi-turn split-conductor transmission-line resonators, Magnetic Resonance in Medicine 38 (1997) 687–689.
[19] J. Fang, M.S. Chow, K.C. Chan, K.K. Wong, G.X. Shen, E. Gao, E.S. Yang, Q.Y. Ma, Design of superconducting MRI surface coil by using method of moment, IEEE Transactions on Applied Superconductivity 12 (2002) 1823–1827.
[20] E.Z. Gao, Q.Y. Ma, A refined circuit model of high temperature superconducting spiral coils for MRI, IEEE Transactions on Applied Superconductivity 11 (2001) 403–406.
[21] S. Serfaty, L. Darrasse, S. Kan, Double-bracelet resonator Helmholtz probe for NMR experiments, Review of Scientific Instruments 66 (1995) 5522–5526.
[22] J.R. Miller, S.E. Hurlston, Q.Y. Ma, D.W. Face, D.J. Kountz, J.R. MacFall, L.W. Hedlund, G.A. Johnson, Performance of a high-temperature superconducting probe for in vivo microscopy at 2.0 T, Magnetic Resonance in Medicine 41 (1999) 72–79.
[23] G.A. Johnson, G.P. Cofer, B. Fubara, S.L. Gewalt, L.W. Hedlund, R.R. Maronpot, Magnetic resonance histology for morphologic phenotyping, Journal of Magnetic Resonance Imaging 16 (2002) 423–429.
[24] G.A. Johnson, G.P. Cofer, S.L. Gewalt, L.W. Hedlund, Morphologic phenotyping with MR microscopy: the visible mouse, Radiology 222 (2002) 789–793.
[25] L. Darrasse, G. Kassab, Quick measurement of NMR-coil sensitivity with a dual-loop probe, Review of Scientific Instruments 64 (1993) 1841–1844.
[26] R.D. Black, T.A. Early, G.A. Johnson, Performance of a high-temperature superconducting resonator for high-field imaging, Journal of Magnetic Resonance Series A 113 (1995) 74–80.
[27] G.A. Johnson, A. Ali-Sharief, A. Badea, J. Brandenburg, G. Cofer, B. Fubara, S. Gewalt, L.W. Hedlund, L. Upchurch, High-throughput morphologic phenotyping of the mouse brain with magnetic resonance histology, Neuroimage 37 (2007) 82–89.
[28] Y. Otake, K. Kose, T. Haish, A solution to the dynamic range problem in MRI using a parallel image acquisition, Concepts in Magnetic Resonance Part B-Magnetic Resonance Engineering 29B (2006) 161–167.